Isotopic dependence of nuclear temperatures

Jun Su[1,2] and Feng-Shou Zhang[1,2,3,*]

[1]*The Key Laboratory of Beam Technology and Material Modification of Ministry of Education, College of Nuclear Science and Technology,*
Beijing Normal University, Beijing 100875, China
[2]*Beijing Radiation Center, Beijing 100875, China*
[3]*Center of Theoretical Nuclear Physics, National Laboratory of Heavy Ion Accelerator of Lanzhou, Lanzhou 730000, China*

A systematic study of isotope temperatures has been presented for heavy-ion collisions at 600 MeV/nucleon via the isospin-dependent quantum molecular dynamics model in the company of the statistical decay model (GEMINI). We find that the isospin dependence of the isotope temperatures in multifragmentation is weak; however, this effect is still visible over a wide isotopic range. The isotope temperatures for the neutron-rich projectiles are larger than those for the neutron-poor projectiles. We also find that the isotope temperatures calculated by the model decrease with increasing nuclear mass.

The concept of a nuclear temperature has been introduced some seventy years ago [1,2]. During the past two decades, many experiments were committed to measuring the nuclear temperatures in multifragmentation [3–7]. The early work was that Pochodzalla *et al.* [8], which gave the caloric curve employing the isotopic thermometer suggested by Albergo [9]. For the slope thermometer, the temperature was obtained from Maxwell-Boltzmann fits to the kinetic energy spectra of the light fragments [10,11]. It was discussed that the slope temperature not only reflects the thermal properties of the multifragmenting system, but also reflects the collective energies coming from the dynamics of the nuclear collision [12,13]. Another method that extracts the temperature from the population of excited states was also adopted [14,15]. For the systems already studied, the limiting temperatures represented by the plateaus of the caloric curve decrease with increasing nuclear mass [16]. One expected that a significant isotopic dependence of the caloric curve or the nuclear temperatures could be measured with radioactive beams [3,5,6].

On the other hand, a large number of theoretical methods have been used to investigate the thermodynamic properties of hot nuclei. The early theoretical work explored the thermal properties of finite nuclei by the temperature-dependent Hartree-Fock model [17]. After that, some microscopic methods [18–23] were developed to investigate the upper limiting temperatures of the nuclear stability and Coulomb instability. The statistical models were found to be very useful for predicting the caloric curve [24]. At the same time, many attempts had already been made to explore the isotopic dependence of the nuclear temperatures [18,21–24]. The early work with the hot liquid-drop model predicted the existence of the limiting temperatures, which showed size effects, Coulomb effects, and significant isospin asymmetry effects [18]. Starting from the temperature-dependent Thomas-Fermi approximation with the effective SkM force, Kolomietz *et al.* found that the plateau temperatures on the caloric curve are almost insensitive to

a change in the asymmetry parameter [21]. Within the same theoretical framework, but for the SBM effective interaction, the caloric curves for isobaric ^{150}Sm and ^{150}Cs were found to be similar [22]. However, the plateau temperature resulting from the multifragmentation of the neutron-poor source (^{124}La) was, by the statistical multifragmentation model, found to be slightly lower by about 0.4 MeV than that for ^{124}Sn and ^{197}Au [24]. The weak asymmetry dependence of the caloric curve for mononuclear configurations was also found [23]. Recently, the isotope temperatures of ^{124}Sn fragmentation were found to exceed those for the neutron-poor systems from the ALADIN experimental data [5–7]. However, the isotopic dependence of the nuclear temperatures is not yet fully understood due to a lack of experimental data and systematic analysis.

In this paper, we attempt to study the isospin effects of the temperatures within a dynamic model. We perform a systematic study for multifragmentation in the mass range of $A = 36$ to 224. Several global fragmentation observables, including the charge distributions, the Z_{bound} distributions, and the charge correlations, are calculated. The isospin effect and the mass effect of the isotope temperatures are discussed.

The isospin-dependent quantum molecular dynamics (IQMD) model [25,26] has been applied successfully in analyzing a large number of observables in heavy-ion collisions at intermediate energies. In a recent publication [27] we performed a study for multifragmentation via the IQMD model incorporating the statistical decay model GEMINI. We will focus on the isotopic dependence of nuclear temperatures in the present work.

The N/Z dependence of the projectile fragmentation of ^{107}Sn, ^{124}Sn, and ^{124}La on ^{nat}Sn at 600 MeV/nucleon has been studied by the ALADIN Collaboration [7]. Here, we adopt ^{120}Sn as targets. The fragment cross sections are shown in Fig. 1. Figure 1(a) shows the charge distributions. From the figure we can see that the main features of the experimental charge distributions are as follows:

  (i) An exponentially decreasing yield of the fragments with increasing charge appears in the region $Z_f < 20$.

  (ii) There is a plateau of rather constant cross sections in the region $20 < Z_f < 40$.
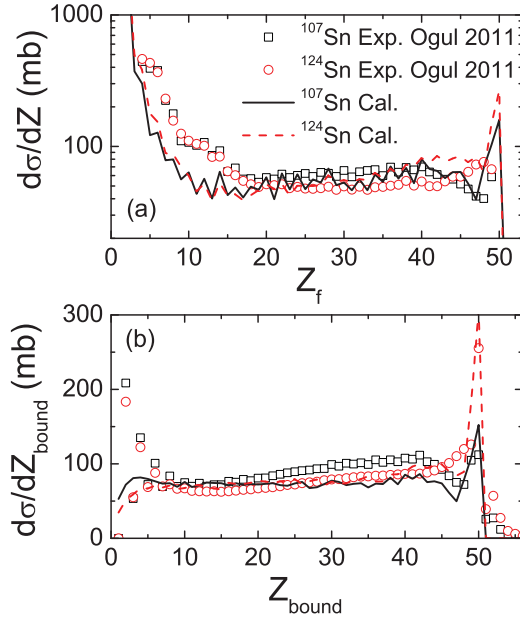
*Corresponding author: fszhang@bnu.edu.cn

FIG. 1. (Color online) Charge (a) and Z_{bound} (b) distributions for reactions of ^{107}Sn + ^{120}Sn and ^{124}Sn + ^{120}Sn at 600 MeV/nucleon. Experimental data are taken from Ogul *et al.* [7].
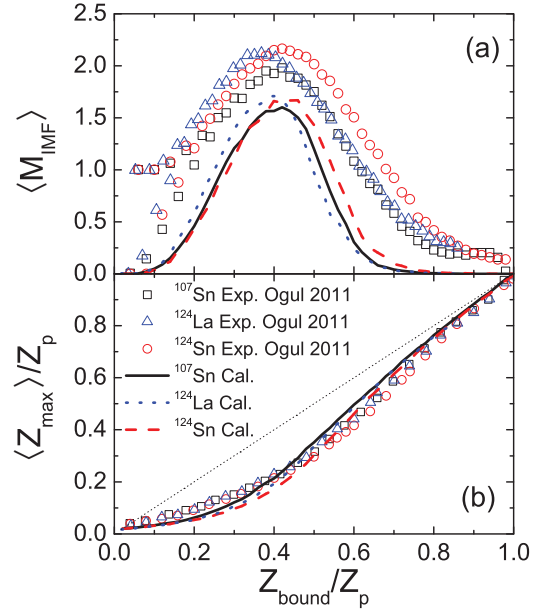

FIG. 2. (Color online) Mean multiplicity of intermediate-mass fragments (a) and mean maximum charge with normalization with Z_p (b) as a function of Z_{bound}/Z_p for reactions of ^{107}Sn + ^{120}Sn, ^{124}La + ^{120}Sn, and ^{124}Sn + ^{120}Sn at 600 MeV/nucleon. Experimental data are taken from Ogul *et al.* [7].

(iii) The rather different trends for the two projectiles are seen in the region $Z_f > 40$. The cross sections for the ^{124}Sn projectile increase with increasing Z_f. For the ^{107}Sn projectile, the cross sections decrease slowly with increasing Z_f.

The behavior of the calculated cross sections is generally in agreement with the data. The main discrepancies of the calculations compared with the experimental data are an underestimation of the charge yields in the region $Z < 20$.

The quantity Z_{bound}, which is defined as the sum of the fragment charge of all fragments with $Z_i \geqslant 2$, is chosen as the principal variable for event sorting. The cross sections as a function of Z_{bound} are shown in Fig. 1(b). For small Z_{bound} (below $Z_{bound} = 10$), the cross sections strongly stagger. This Z_{bound} range corresponds to the vaporization events, in which several αs are produced. For the middle values of Z_{bound}, the cross sections vary rather smoothly with Z_{bound}. For Z_{bound} toward the projectile charge Z_p, the dropping of the cross sections in the ^{107}Sn case is noticed, while it rises for ^{124}Sn. A good agreement is observed between the experimental data and the calculations.

We show the $\langle M_{IMF} \rangle$-Z_{bound} scaling with normalization by Z_p in Fig. 2(a). We can see that the multiplicities exhibit the universal rise and fall of the fragment production. Experimentally, the peak positions of M_{IMF} are $Z_{bound}/Z_p = 0.42$, 0.42, 0.39 for the projectiles of ^{107}Sn, ^{124}Sn, and ^{124}La, respectively, while the peak positions of the calculations are $Z_{bound}/Z_p = 0.42$, 0.36, 0.38, respectively. The peak positions are well reproduced by the simulations, but deviations occur at the peak values. The mean multiplicities of the intermediate mass fragments (IMFs) calculated by the model are smaller than those in the experiment. However, for the

following discussion of the isospin effect, the peak positions of the $\langle M_{IMF} \rangle$-Z_{bound} scaling and the relationship between the $\langle M_{IMF} \rangle$ values for different reactions are more significant than the $\langle M_{IMF} \rangle$ values.

In Fig. 2(b) we show the $\langle Z_{max} \rangle/Z_p - Z_{bound}/Z_p$ correlation. With increasing Z_{bound}/Z_p, the average charge of the heaviest fragment first slowly rises and then strongly increases, closing to the line of $\langle Z_{max} \rangle/Z_p = Z_{bound}/Z_p$ at the end. The transition from predominantly residue production to multifragmentation appears as a reduction of $\langle Z_{max} \rangle/Z_p$ with respect to Z_{bound}/Z_p, which occurs between $Z_{bound}/Z_p = 0.6$ to 0.8. The agreement between theory and experiment is very satisfactory overall and sufficient for performing the following analysis in individual intervals of Z_{bound}/Z_p.

In order to give a systematic analysis of the isospin effect and the mass effect of the isotope temperatures, we perform a systematic study for the multifragmentation in a wide mass range and a wide isotopic range. The T_{HeLi} thermometer that based on the ^{3}He/^{4}He and ^{6}Li/^{7}Li yield ratios is adopted in the present work.

$$T_{HeLi} = (13.3 \text{ MeV})/\ln\left(2.2\frac{Y_{^6Li}/Y_{^7Li}}{Y_{^3He}/Y_{^4He}}\right). \qquad (1)$$

In Fig. 3, the isotope temperatures are displayed as a function of the normalized Z_{bound} by Z_p for the reactions ^{107,124}Sn, ^{124}La + ^{120}Sn, ^{176,192,208,224}Pb + ^{40}Ca, ^{78,94,110}Zr + ^{40}Ca, and ^{36,44,52}Ca + ^{40}Ca at 600 MeV/nucleon. The experimental data for ^{107,124}Sn, ^{124}La + ^{nat}Sn at 600 MeV/nucleon from Ref. [6] are also shown in Fig. 3(a). For the experimental data, the temperatures of ^{124}Sn fragmentation are slightly larger than those of the neutron-poor systems (^{107}Sn and ^{124}La). The temperatures for the bin of $Z_{bound}/Z_p = 0.1$ are
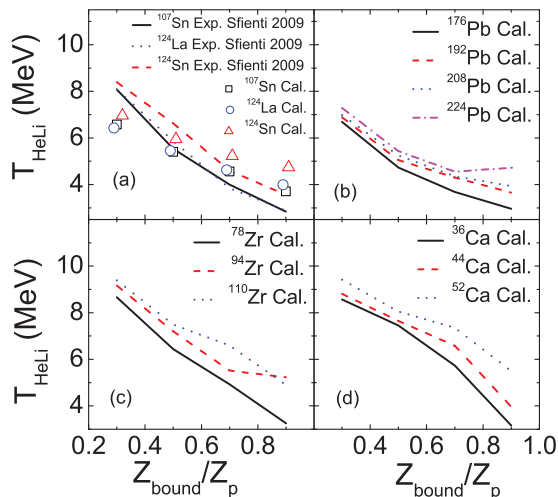
FIG. 3. (Color online) T_{HeLi} as a function of Z_{bound}/Z_p for reactions of ^{107,124}Sn, ^{124}La + ^{120}Sn, ^{176,192,208,224}Pb + ^{40}Ca, ^{78,94,110}Zr + ^{40}Ca, and ^{36,44,52}Ca + ^{40}Ca at 600 MeV/nucleon. Experimental data are taken from Sfienti et al. [6].

not shown in the figure due to the large statistical uncertainties. It can be seen from Fig. 3(a) that the isotope temperatures by the model follow the trend of the experimental data. However, the magnitudes of the calculated isotope temperatures for all projectiles show discrepancies with the experimental data. For the bins at small Z_{bound}, the calculated isotope temperatures overestimate the experimental data by about 2 MeV. For the bins at $Z_{bound}/Z_p = 0.7, 0.9$, the calculated magnitudes are smaller than the experimental data by about 1 MeV. It seems that the calculations reproduce isotopic dependence of the isotope temperatures, although the isotopic dependence is rather weak. The temperatures of two neutron-poor systems (^{107}Sn and ^{124}La) are roughly equal, which are exceeded by those of ^{124}Sn by about 0.5 MeV. In Table I, we show the mean temperature differences between the neutron-rich and neutron-poor systems both for the calculations and the experimental data:

$$\Delta T = T_{^{124}Sn} - \frac{T_{^{107}Sn} + T_{^{124}La}}{2}. \quad (2)$$

We can see from Table I that the calculated result for $Z_{bound}/Z_p = 0.5$ is twice as large as the experimental result. Apart from this, the differences between the calculations and the experimental data are within 15%. It seems that this model reproduces the experimental isotopic dependence of the temperatures.

TABLE I. Mean temperature differences between neutron-rich and neutron-poor systems.

	Z_{bound}/Z_p			
	0.3	0.5	0.7	0.9
ΔT_{expt} (MeV)[a]	0.46	0.52	0.63	0.89
ΔT_{calc} (MeV)	0.45	0.93	0.72	0.75

[a]Ref. [11]

For Pb, Zr, and Ca projectiles, the temperatures also show the general trend of decreasing with increasing Z_{bound}/Z_p. The temperatures of Pb projectiles [Fig. 3(b)] increase with decreasing Z_{bound} from $T = 3$ MeV to about 7 MeV, within the range of the earlier experimental measurement of ^{197}Au fragmentations [28]. The temperatures of Zr and Ca projectiles [Figs. 3(c) and 3(d)] for the bin of $Z_{bound}/Z_p = 0.3$ are about 9 MeV, which are larger than those of Sn and Pb. There are slight fluctuations in the smooth trend for Zr and Ca projectiles. This is due to the fact that, with the same simulation events, the intermediate-mass fragments are produced more abundantly for heavy projectiles than for light projectiles. We also find that the temperatures for the neutron-rich projectiles are larger than those for the neutron-poor projectiles for Pb, Zr, and Ca projectiles. The difference of the temperatures for the bin of $Z_{bound}/Z_p = 0.5$ between the very-neutron-rich projectiles and the very-neutron-poor projectiles are 0.70, 1.05, and 0.59 MeV for Pb, Zr, and Ca, respectively. It seems that the isospin effect for Zr is the strongest.

To further investigate the isotopic dependence of the isotope temperatures and show the mass effect, we display in Fig. 4 the T_{HeLi} temperatures that were derived from isotopic yields for $0.2 < Z_{bound}/Z_p < 0.6$ as a function of the neutron-to-proton ratio N/Z. This value of Z_{bound} corresponds to the regime of multifragmentation (see Fig. 2). It is clear that the isotope temperatures increase monotonically with the neutron-to-proton ratio N/Z. Comparing to the early works, we find that the global behavior of the isotopic-dependent nuclear temperatures is in good agreement with that of the experimental data [6], the calculations by the statistical multifragmentation model [24], and those for mononuclear configurations [23]. The differences of the isotope temperatures between the very-neutron-rich projectiles and the very-neutron-poor projectiles reach 0.65 MeV for ^{36}Ca and ^{52}Ca and to 0.72 MeV for ^{176}Pb and ^{224}Pb.

The mass effect of the temperatures could be seen in Fig. 4. The highest temperature is observed for Ca projectiles and the lowest temperature for Pb projectiles, with Zr and Sn in between. The temperatures decrease with increasing mass. It has previously been suggested that the limiting temperatures calculated from the temperature-dependent Hartree-Fock model [18] and the plateau temperatures on the experimental caloric curve [16] show the similar mass effect. Song et al. [20]
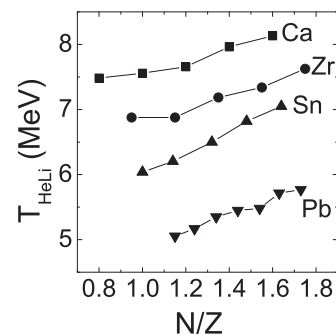

FIG. 4. T_{HeLi} derived from isotopic yields for $0.2 < Z_{bound}/Z_p < 0.6$ as a function of neutron-to-proton ratio N/Z for reactions of Ca, Zr, Sn, and Pb isotopes on ^{40}Ca at 600 MeV/nucleon.

explained that the mass effect is caused by the Coulomb interaction because the system with larger A (and hence larger Z) has larger Coulomb pressure, which makes the system easy to separate.

In conclusion, via the IQMD model in the company of the GEMINI model, we have presented a systematic study of the isotope temperatures for heavy-ion collisions at 600 MeV/nucleon. The isotope temperatures, which are derived from double ratios of helium and lithium isotopic yields, show a smooth fall with increasing Z_{bound} for all reactions. We find that the temperatures for the neutron-rich projectiles are larger than those for the neutron-poor projectiles. The isospin dependence of the isotope temperatures in multifragmentation is weak but can still be visible over a wide isotopic range. The mass effect of the isotope temperatures, which decreases with increasing projectile mass, is similar to that of the limiting temperatures in Ref. [18] and the plateau temperatures in Ref. [16]. A natural extension of the present study would be to probe the isospin features in the early stage of the collision. This exploration should be instructive for understanding the isospin dependence of the nuclear temperatures.

[1] H. A. Bethe, Rev. Mod. Phys. **9**, 69 (1937).

[2] V. F. Weisskopf, Phys. Rev. **52**, 295 (1937).

[3] A. Kelić, J. B. Natowitz, and K.-H. Schmidt, Eur. Phys. J. A **30**, 203 (2006).

[4] J. B. Natowitz, R. Wada, K. Hagel, T. Keutgen, M. Murray, A. Makeev, L. Qin, P. Smith, and C. Hamilton, Phys. Rev. C **65**, 034618 (2002).

[5] W. Trautmann *et al.*, Int. J. Mod. Phys. E **17**, 1838 (2008).

[6] C. Sfienti *et al.*, Phys. Rev. Lett. **102**, 152701 (2009).

[7] R. Ogul *et al.*, Phys. Rev. C **83**, 024608 (2011).

[8] J. Pochodzalla *et al.*, Phys. Rev. Lett. **75**, 1040 (1995).

[9] S. Albergo, S. Costa, E. Costanzo, and A. Rubbino, Nuovo Cimento A **89**, 1 (1985).

[10] G. D. Westfall, Phys. Lett. B **116**, 118 (1982).

[11] B. V. Jacak, G. D. Westfall, C. K. Gelbke, L. H. Harwood, W. G. Lynch, D. K. Scott, H. Stöcker, M. B. Tsang, and T. J. M. Symons, Phys. Rev. Lett. **51**, 1846 (1983).

[12] T. Odeh *et al.*, Phys. Rev. Lett. **84**, 4557 (2000).

[13] L. W. Chen, F. S. Zhang, G. M. Jin, and Z. Y. Zhu, Phys. Lett. B **459**, 21 (1999).

[14] D. J. Morrissey, W. Benenson, E. Kashy, B. Sherrill, A. D. Panagiotou, R. A. Blue, R. M. Ronningen, J. van der Plicht, and H. Utsunomiya, Phys. Lett. B **148**, 423 (1984).

[15] J. Pochodzalla *et al.*, Phys. Rev. Lett. **55**, 177 (1985).

[16] J. B. Natowitz, K. Hagel, Y. Ma, M. Murray, L. Qin, R. Wada, and J. Wang, Phys. Rev. Lett. **89**, 212701 (2002).

[17] P. Bonche, S. Levit, and D. Vautherin, Nucl. Phys. A **427**, 278 (1984).

[18] J. Besprosvany and S. Levit, Phys. Lett. B **217**, 1 (1989).

[19] J. B. Natowitz *et al.*, Phys. Rev. Lett. **104**, 202501 (2010).

[20] H. Q. Song and R. K. Su, Phys. Rev. C **44**, 2505 (1991).

[21] V. M. Kolomietz, A. I. Sanzhur, S. Shlomo, and S. A. Firin, Phys. Rev. C **64**, 024315 (2001).

[22] S. K. Samaddar, J. N. De, X. Viñas, and M. Centelles, Phys. Rev. C **76**, 041602 (2007).

[23] C. Hoel, L. G. Sobotka, and R. J. Charity, Phys. Rev. C **75**, 017601 (2007).

[24] R. Ogul and A. S. Botvina, Phys. Rev. C **66**, 051601 (2002).

[25] J. Aichelin, Phys. Rep. **202**, 233 (1991).

[26] C. Hartnack, Z. X. Li, L. Neise, G. Peilert, A. Rosenhauer, H. Sorge, J. Aichelin, H. Stöcker, and W. Greiner, Nucl. Phys. A **495**, 303 (1989).

[27] J. Su, F. S. Zhang, and B. A. Bian, Phys. Rev. C **83**, 014608 (2011).

[28] H. F. Xi *et al.*, Z. Phys. A **359**, 397 (1997).